# Simulating a two-dimensional time dependant Schrödinger equation by using the Crank-Nicolson method

Fuad Dadvar — Duncan Wilkins — Don Philip Bullecer — Erling Nupen
Department of Physics, University of Oslo, Norway
https://github.com/dondondoooooon/DONFYS3150

December 15, 2021

**Abstract**

In this article, the study of the time dependent Schrödinger equation through a non-slit and multiple-slit box setup, has been performed. The method utilized is the Crank Nicolsen method. Through all the box setups a diffraction pattern is observed. It has been found that the probability density of the Schrödinger equation is denser at an initial time $t = 0$ and then starts to propagate until it reaches a high potential barrier at $t = 0.002$, where it scatters. The total probability of the probability function $p_{ij}^n = 1$ should be conserved over time. However, the numerical values show that there are small deviations from 1. The deviation for a non-slit box setup were found to be $Min = -1.821 \cdot 10^{-14}$ , $Max = 1.145 \cdot 10^{-13}$, $Mean = 1.740 \cdot 10^{-14}$, $Standard = 3.488 \cdot 10^{-14}$. And for a double-slit box setup, the deviation were found to be $Min = -2.487 \cdot 10^{-14}$, $Max = 1.665 \cdot 10^{-14}$, $Mean = -6.625 \cdot 10^{-15}$, $Standard = 6.6720 \cdot 10^{-15}$. This behaviour is caused by round off errors as a consequence of utilizing a finite algorithm, as well as the nature of the chosen matrix equation solver. Snapshots of the wave equation propagating through the $xy$ grid, as well as it's 2D probability function, for a double-slit setup are also plotted and observed. Propagation, collision, and reflection of the wave function was observed. It has further been observed that the Schrödinger equation for the different box-setup for a given time $t$ and position $x$ along the $y$ axis created a 3 different diffraction patterns.

# Contents

# 1 Introduction

The aim of this article is to simulate the time dependent Schrödinger equation in a system of two dimensional position space and one dimensional time-space. The solution to the Schrödinger equation can be interpreted as a complex valued wave-function. This wave-function has no physical meaning, but the wave-function squared can be interpreted as a probability density of the particle to be at some point in space-time. We will simulate the Schrödinger equation by using the Crank-Nicolson method in a 2 spatial dimensions plus one time dimension.

Thereby we simulate how the probability density of the particle to be somewhere in space-time when the system evolves with time. We will simulate the probability density when the particle goes through different slit-in-a-box setups. For any given time, we expect that the probability is a conserved quantity equal to one. The probability density is given by the Born rule, which is needed since the exact position of the particle is limited by the Heisenberg-Principle.

# 2 Theory

## 2.1 The Schrodinger Equation

The quantum state $|\psi\rangle$ is a vector in Hilbert space, $\mathcal{H}$. The formulation of Schrodinger's equation in Hilbert space can be generalized to the time-dependent Schrodinger equation

$$i\hbar\frac{d}{dt}|\Psi\rangle = \hat{H}|\Psi\rangle\,. \tag{1}$$

Where $\hat{H}$ is the Hamiltonian operator, $\hat{H} = \frac{\hat{p}^2}{2m} + V(\hat{x})$. Where $\hat{p}/2m$ is the kinetic energy of the system, m is the mass of the system we are studying, and $\hat{p}$ is the momentum operator. $V(\hat{x})$ is the potential. The Hamiltonian corresponds to the total energy of the system, which for the time-dependent Schrodinger equation evolves over time.

Since wave-functions exists in a completely normelized vector space, a Banach space[1],the inner product is also Hilbert-space, defined as

$$\langle\Phi|\Psi\rangle = \int dx\phi(x,t)^*|\psi(x,t)\,\langle\phi|\psi\rangle$$

Where $\langle\Phi| = |\Phi\rangle^\dagger$ is some end-state of our system. $|\psi\rangle$ is the time-dependent coefficient of the eigenstates of the Hamiltonian. As-well as describing the projection of $\Phi$ onto $\Psi$, this inner-product can also be interpreted as the probability

amplitude of an initial-state $|\Psi\rangle$ to collapse into the state $\langle\Phi|$ upon measuring the state. If we take this final state to be equal the initial state, we get an probability amplitude for the state $\Psi$ to exist

$$P = \langle\Psi|\Psi\rangle = \int dx\psi(x,t)^*\psi(x,t),$$

Where P donates probability for the case of a single, non-relativist particle in two dimensions, working in some abstract vector-space is inconvenient, and we would much rather define our abstract vector as a complex valued wave-function in position space. Here the inner product $\langle\phi|\phi\rangle$ is just one. The probability is a conserved quantity, so if we integrated over all possible space, we would get one, which makes sense because there is a 100 % probability for our particle to be somewhere in space. $\Psi$ in position-space can be expressed as a complex valued function, $\Psi(x,y,t) = \langle x,y|\Psi\rangle$ known as the wave-function. The Schrodinger equation formulated in position space becomes:

$$i\hbar\frac{\partial}{\partial t}\Psi(x,y,t) = -\frac{\hbar^2}{2m}\left(\frac{\partial^2}{\partial x^2} + \frac{\partial^2}{\partial y^2}\right)\Psi(x,y,t) + V(x,y,t)\Psi(x,y,t), \qquad (2)$$

Where the terms $-\frac{\hbar^2}{2m}\frac{\partial^2\Psi}{\partial x^2}$ and $-\frac{\hbar^2}{2m}\frac{\partial^2\Psi}{\partial y^2}$ are recognized as expressions of kinetic energy, with $m$ being the particle mass. In position space, the Born rule, which is equal to probability amplitude in abstract vector space becomes:

$$p(x,y;t) = |\Psi(x,y,t)|^2 = \Psi^*(x,y,t)\Psi(x,y,t). \qquad (3)$$

Where $p(x,y;t)$ designates the probability density of detecting a particle at position $(x,y)$ at some time $t$.

## 2.2 Crank-Nicolsen for 2D function

The Crank-Nicolsen method is an average of an explicit method the forward time scheme, which is conditionally stable and an implicit method, the backward time scheme that is always unconditionally stable. The Crank Nicolson is therefor unconditionally stable and solves a tri-diagonal matrix at each time step. We essentially do an Euler method to simulate the time step. We take the second order derivation in time, and the second order derivative in space. The difference in time becomes second order in the $n/n+1$ and in the space $i,j/i+1,j+1$. The time and space stepping both become of second order. We write the Crank-Nicolsen method for two dimension as:

$$u_{i,j}^{n+1} - r[u_{i+1,j}^{n+1} - 2u_{i,j}^{n+1} + u_{i-1,j}^{n+1}] - r[u_{i,j+1}^{n+1} - 2u_{i,j}^{n+1} + u_{i,j-1}^{n+1}] + \frac{i\Delta t}{2}v_{i,j}u_{i,j}^{n+1}$$

$$= \mathrm{u}^n_{i,j} - r[u^n_{i+1,j} - 2u^n_{i,j} + u^n_{i-1,j}] - r[u^n_{i,j+1} - 2u^n_{i,j} + u^n_{i,j-1}] + \frac{i\Delta t}{2} v_{i,j} u^n_{i,j} (4)$$

Where $r = \frac{i\Delta t}{2h^2}$. This is stable for all choices of $\Delta t, \Delta x, \Delta y$.

[2] We use Dirichlet boundary conditions such that our function only propagates within the boundary points, and our boundary points are given as:

$$\begin{aligned} u(x = 0, y, t) &= 0, \\ u(x = 1, y, t) &= 0, \\ u(x, y = 0, t) &= 0, \\ u(x, y = 1, t) &= 0. \end{aligned}$$

### 2.2.1 Matrix Equation

In applying the Crank-Nicolson method in 2D, we must be able to refer to the neighbouring positions $u^n_{i+1,j}$, $u^n_{i-1,j}$, $u^n_{i,j+1}$, and $u^n_{i,j-1}$ for a given position in $u^n_{ij}$.

Taking into account the boundary condition, as well as the discretized Schrondinger equation, we are able to express the equation 2.2 in matrix form as

$$A\vec{u}^{n+1} = B\vec{u}^n. \tag{5}$$

Where the vectors $\vec{u}^{n+1}$ and $\vec{u}^n$ are column vectors containing the $u^n_{ij}$ for all the internal points of the $xy$ grid at time step $n$.

$A$ and $B$ matrices for a given 3x3 $u^n_{ij}$ matrix are written as

$$A = \begin{bmatrix} a_0 & -r & 0 & -r & 0 & 0 & 0 & 0 & 0 \\ -r & a_1 & -r & 0 & -r & 0 & 0 & 0 & 0 \\ 0 & -r & a_2 & 0 & 0 & -r & 0 & 0 & 0 \\ -r & 0 & 0 & a_3 & -r & 0 & -r & 0 & 0 \\ 0 & -r & 0 & -r & a_4 & -r & 0 & -r & 0 \\ 0 & 0 & -r & 0 & -r & a_5 & 0 & 0 & -r \\ 0 & 0 & 0 & -r & 0 & 0 & a_6 & -r & 0 \\ 0 & 0 & 0 & 0 & -r & 0 & -r & a_7 & -r \\ 0 & 0 & 0 & 0 & 0 & -r & 0 & -r & a_8 \end{bmatrix},$$

and

$$B = \begin{bmatrix} b_0 & r & 0 & r & 0 & 0 & 0 & 0 & 0 \\ r & b_1 & r & 0 & r & 0 & 0 & 0 & 0 \\ 0 & r & b_2 & 0 & 0 & r & 0 & 0 & 0 \\ r & 0 & 0 & b_3 & r & 0 & r & 0 & 0 \\ 0 & r & 0 & r & b_4 & r & 0 & r & 0 \\ 0 & 0 & r & 0 & r & b_5 & 0 & 0 & r \\ 0 & 0 & 0 & r & 0 & 0 & b_6 & r & 0 \\ 0 & 0 & 0 & 0 & r & 0 & r & b_7 & r \\ 0 & 0 & 0 & 0 & 0 & r & 0 & r & b_8 \end{bmatrix}.$$

Where $a_k$ and $b_k$ are vectors of $(M-2)^2$ length, that are defined as:

$$a_k = 1 + 4r + \frac{i\Delta t}{2} v_{ij} \tag{6}$$

$$b_k = 1 - 4r - \frac{i\Delta t}{2} v_{ij} \tag{7}$$

More generally, for a given axis with $M$ number of points, our system matrix $u_{ij}^n$ will have the dimensions $(M-2)$x$(M-2)$. This leads to the corresponding $A$ and $B$ matrices being of dimensions $(M-2)^2$x$(M-2)^2$. Both $A$ and $B$ matrices is built up of smaller submatrices of size $(M-2)$x$(M-2)$, where the diagonal submatrices have the patterns

$$sub(A)_{diag} = \begin{bmatrix} a_0 & -r & 0 & ... & ... & 0 \\ -r & a_1 & -r & 0 & ... & ... \\ 0 & -r & a_2 & -r & 0 & ... \\ ... & 0 & -r & ... & -r & 0 \\ ... & ... & 0 & -r & a_{(M-2)^2-2} & -r \\ 0 & ... & ... & 0 & -r & a_{(M-2)^2-1} \end{bmatrix},$$

and

$$sub(B)_{diag} = \begin{bmatrix} b_0 & r & 0 & ... & ... & 0 \\ r & b_1 & r & 0 & ... & ... \\ 0 & r & b_2 & r & 0 & ... \\ ... & 0 & r & ... & r & 0 \\ ... & ... & 0 & r & b_{(M-2)^2-2} & r \\ 0 & ... & ... & 0 & r & b_{(M-2)^2-1} \end{bmatrix},$$

whilst the upper and lower subdiagonal submatrices $-sub(A)_L = sub(B)_L = sub(B)_U = -sub(A)_U$ have the pattern

$$sub(B)_L = \begin{bmatrix} r & 0 & 0 & ... & ... & 0 \\ 0 & r & 0 & 0 & ... & ... \\ 0 & 0 & ... & 0 & 0 & ... \\ ... & 0 & 0 & ... & 0 & 0 \\ ... & ... & 0 & 0 & r & ... \\ 0 & ... & ... & 0 & 0 & r \end{bmatrix}.$$

# 3 Method

## 3.1 Discretized Schrodinger equation.

Assuming all dimensional valued variables have been scaled away, the Schrodinger equation take the form:

$$i\frac{\partial u}{\partial t} = -\frac{\partial^2 u}{\partial x^2} - \frac{\partial^2 u}{\partial y^2} + v(x,y)u. \tag{8}$$

Where all the variables in equation (8) are dimensionless. With this new notation the Born rule 3, becomes:

$$p(x,y;t) = |u(x,y,t)|^2 = u^*(x,y,t)u(x,y,t) \tag{9}$$

### 3.1.1 Initial State $u_{ij}^0$ and Cube Matrices

We set up our initial state $u_{ij}^0$ based on a normalized Gaussian wavepacket

$$u(x,y,t=0) = e^{-\frac{(x-x_c)^2}{2\sigma_x^2} - \frac{(y-y_c)^2}{2\sigma_y^2} + ip_x(x-x_c) + ip_y(y-y_c)} \tag{10}$$

where the following parameters represent:

- $x_c$ and $y_c$ are the initial centre coordinates of the wavepacket
- $\sigma_x$ and $\sigma_y$ are the initial widths of the wavepacket
- $p_x$ and $p_y$ are the wavepacket momenta.

$x_c$ and $y_c$ are the coordinates of the centre of the initial wavepacket, $\sigma_x$ and $\sigma_y$ are the initial widths

Furthermore, we store all matrices $u_{ij}^n$ for a given time step $n$ in a cube matrix filled of variable type complex_double, such that we have a cube matrix of dimensions $MxMxt_n$ where $t_n$ is the number of time steps that we will iterate.

## 3.2 Applications of Crank-Nicolson method

### 3.2.1 The Potential $V$

We will construct our barrier for our double-slit, single-slit, and triple-slit by setting the value for the elements $v_{ij}$ in $V$ to be extremely high. The parameters of this barrier is as follows:

- Barrier thickness (x-axis): 0.02
- Barrier position (x-axis): 0.5
- Wall piece length separating two slits (y-axis): 0.05
- Slit aperture (y-axis): 0.05

### 3.2.2 Vectorization of Matrices

An essential part of being able to use Crank-Nicolson method on a 2+1 dimension system is being able to represent or express a given $L$x$L$ matrix $u_{ij}^n$ in a single vector $\vec{u}^n$ of length $L^2$. The order of elements inside $\vec{u}$ corresponds to a flattened vector of $u_{ij}^n$ where the columns of $U$ are concatenated.

This can be done by making a function that takes in a pair of indexes $(i, j)$ and returns a single index $k$ which gives the position of $u_{ij}^n$ in the vector $\vec{u}^n$. However, an easier way to implement this is to use a function in Armadillo called '*.as_col()*' that returns a column-wise flattened column vector.

### 3.2.3 Matrix Equation

We find the matrix $A$ and $B$, and then found the next $\vec{u}^{n+1}$ using the current $\vec{u}^n$ This was done by solving a multiplication B$\vec{u}^n$ = b. We implement a solver $SPS.solve$ which is a armadillo solver.

■ Algorithm 1
- Setting up $V$ potential matrix via the parameters.
- Setting up the initial state $U$ via Gaussian wavepacket via the parameters
- Setting initial slice of the cube matrix equal to U
  $cubeS.slice(0) \leftarrow U$
- Vectorize initial $U$ matrix
  $U \leftarrow vectorize(U)$
- Setting up $A$ and $B$ matrix

• **for** $i = 1, 2, \ldots, T_{end}$ **do**
  Matrix multiply $\vec{b} \leftarrow B\vec{u}$
  - Using solver to solve $A\vec{x} = \vec{b}$
    Redefine $\vec{u} \leftarrow \vec{x}$
  - Reshape our vector $\vec{u}$ to a $L \times L$ matrix
    $s \leftarrow mat(u).reshape(L, L)$
    Insert into $cubeS.slice(n+1) \leftarrow s$

# 4 Result and discussion

## 4.1 Total probability of a single particle over time

### 4.1.1 Simulation and deviation without slit-barrier

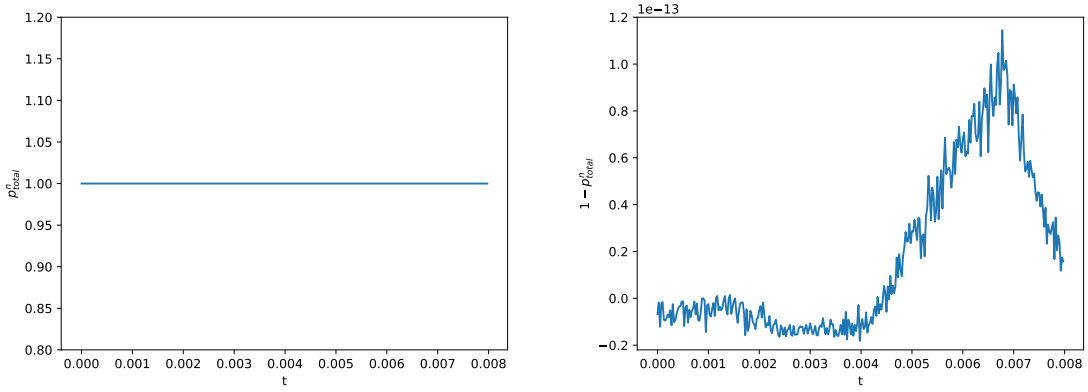


(a) (b)

Figure 1: In the left most plot (a) the integrated probability density of a single particle without any slit barrier is plotted over a time interval $t \in [0, 0.008]$. The right-most plot (b) shows the deviation from the expected total probability of $(p^n_{total} = 1)$ over the same time-interval as in (a).

Table 1: Max, min and mean deviations from the total probability ($p^n_{total} = 1$) over a time interval of $t \in [0, 0.008]$

| | |
|---|---|
| Max. Deviation | $1.145 \cdot 10^{-13}$ |
| Min. Deviation | $-1.821 \cdot 10^{-14}$ |
| Mean deviation | $1.740 \cdot 10^{14}$ |
| Standard deviation | $3.488 \cdot 10^{14}$ |

Figure (1)(a) shows that the probability density of a single particle at any given time $n$ is equal to 1. This to be expected since the total probability density when integrated over all space is a conserved quantity equal to 1. The plot in 1(b) shows that the deviations increases with time, which physically does not make sense as the total probability in the probability function $p^n_{ij}$ is always equal to one for all time steps, i.e. a conserved a quantity. However, these small deviations can be caused by the method we used for solving the matrix equation 2.2.1, as well as, due to both round-off and numerical truncation error. We see the farther we iterate in time in the no-slit-configuration, the greater the deviation becomes relatively speaking.

#### 4.1.2 Simulation and deviation with double-slit-barrier

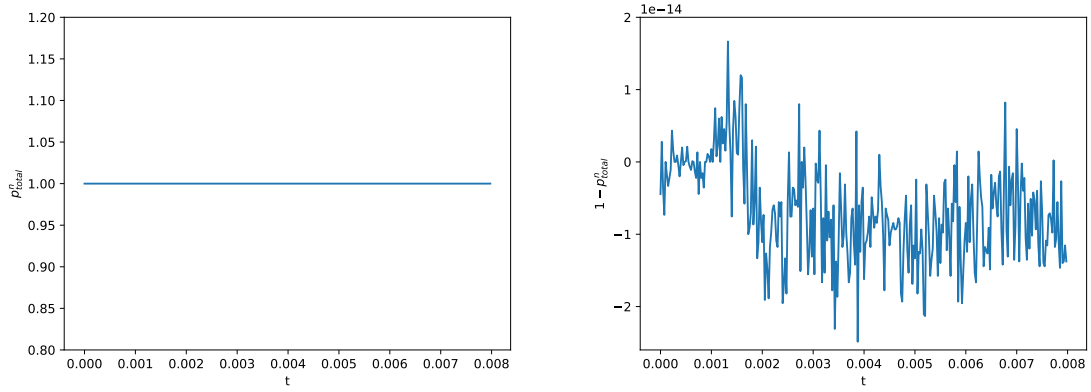


(a) (b)

Figure 2: In the left most plot (a) the integrated probability density of a single particle with double slit barrier set-up is plotted over a time interval of zero seconds to eight milliseconds. The right-most plot (b) shows the deviation from the expected total probability of one over the same time-interval as in (a).

The integrated probability density is trivially one in both the double slit set-up and no-slit set-up. There is a clear difference in the deviation plot of the double and non-slit set-ups. However, the double slit deviation plot is a fac-

Table 2: Max, min and mean deviations from the total probability of one over a time interval of zero to eight milliseconds with a double-slit.

| | |
|---|---|
| Max. Deviation | $1.665 \cdot 10^{-14}$ |
| Min. Deviation | $-2.487 \cdot 10^{-14}$ |
| Mean deviation | $-6.625 \cdot 10^{-15}$ |
| Standard deviation | $6.720 \cdot 10^{-15}$ |

tor 10 smaller, since the y-axis is scaled by 1e-14, whilst the no-slit deviation plot is scaled by 1e-13. So upon a closer inspection, the truncation error after about 4 milliseconds quickly rises to a maximum of 12e-14, which is far greater than that of the double slit set-up which is reasonably stable around a -1e14 deviation.

## 4.2 Time evolution of the 2D probability function

### 4.2.1 For multiple t

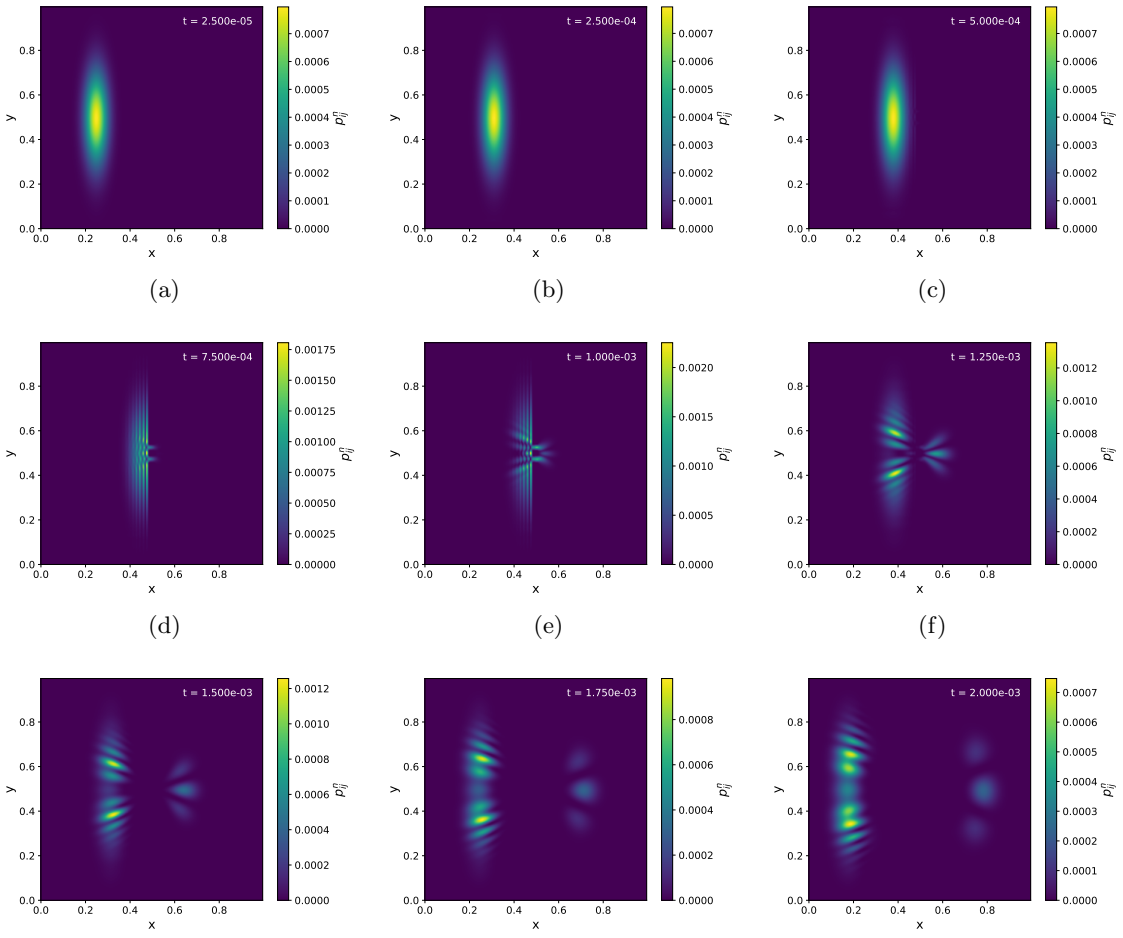


Figure 3: This figure shows us 9 different subplots of a 2D probability function. We see that the position of the particle in the $x, y$ - plane can be observed due to total probability density for multiple timeframes. Where our $t = [0, 0.002]$ where we jump 0.00025 in between each subplot. On the left side of each subplot we can also see the probability density as it increases upwards along the $y$-axis

From the color-bar scheme, the first contour plot show an high probability of finding an initial particle at $x = 0.25, y = 0.50$ and as time progresses we see the particle being reflected as-well as creating an interference pattern as it

goes through the slit. The first three plots show a high probability of finding the particle at $y = 0.5$, whilst the particle move to right. In plot (d), as the particle approaches the double slit, the probability density appears more wave-like, which is reasonable to assume comes from the wave-particle duality of the particle. As these probability density waves goes through the slits, some of them overlap, creating interference patterns clearly seen in plots (f) through (i). The dark spots between the wave is where they negatively interfere.

### 4.2.2 Real and Imaginary part of $u_{ij}^n$

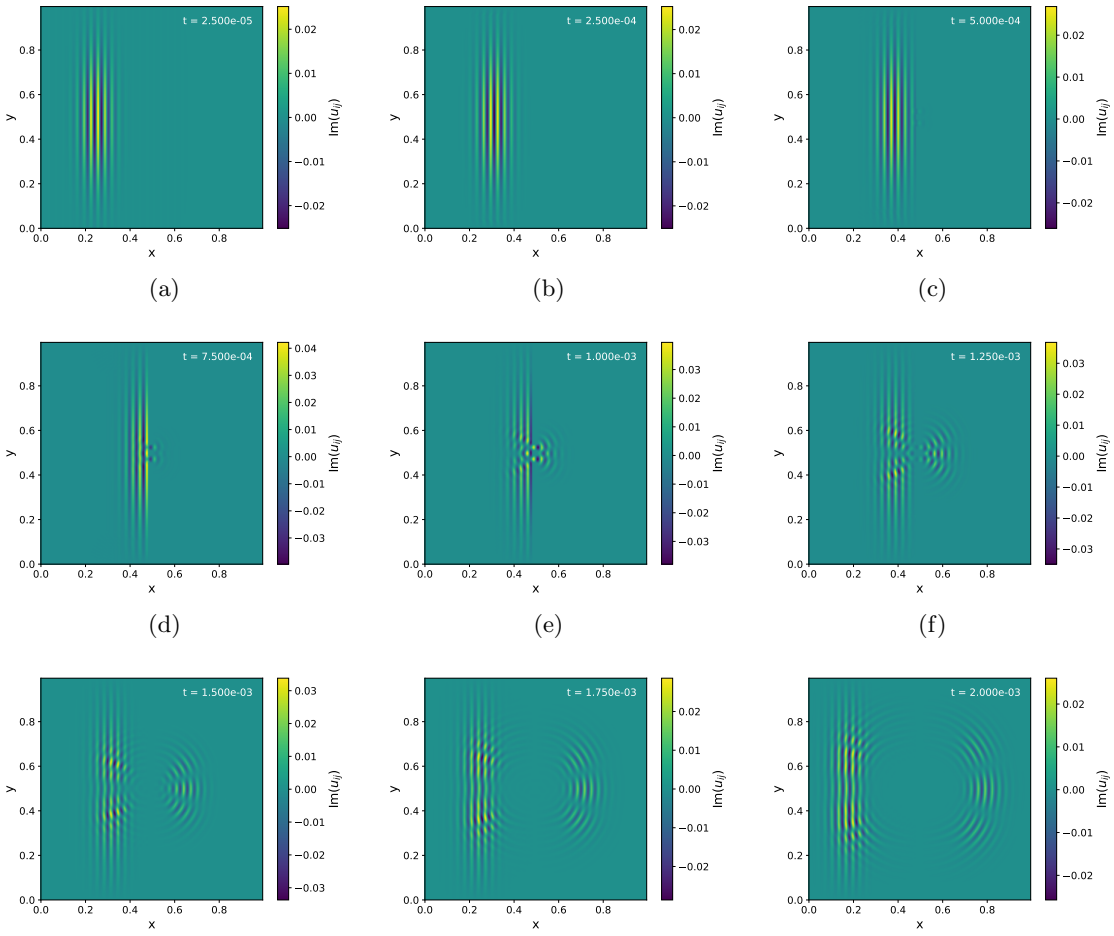


(a) (b) (c)

(d) (e) (f)

(g) (h) (i)

Figure 4: Snapshots of the imaginary part of the wave function $u_{ij}$ at 9 different time steps.

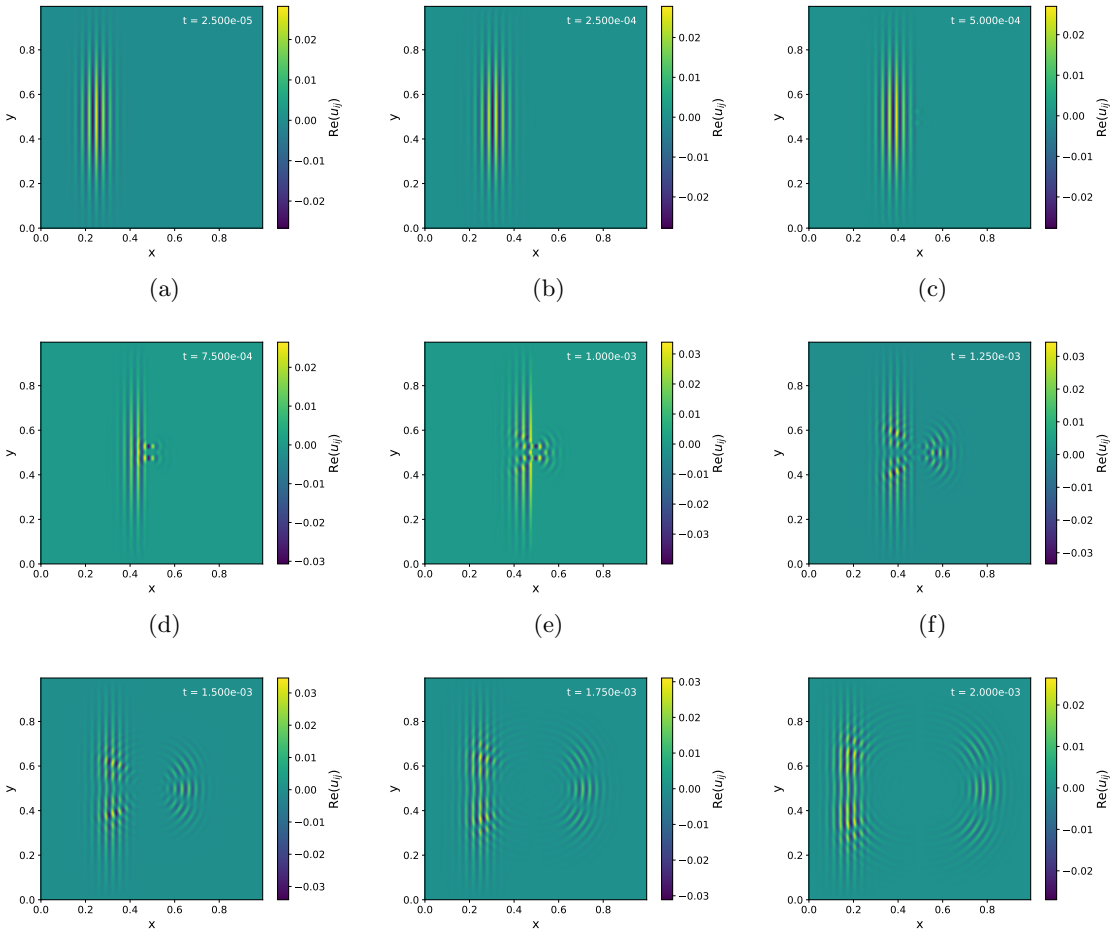


Figure 5: Snapshots of the real part of the wave function $u_{ij}$ at 9 different time steps.

We observe that both the real and imaginary part of the wave function are very similar. As shown in Figure (5).(a) it starts at the left side of the $x, y$ grid at $t = 0$, and as time evolves it propagates towards the center until it meets the double slit wall and then reflects off the wall. The collision with the wall causes some scattering of the wave function as shown in the Figures 5.(d)-(i). But it is observed in Figure 5.(g)-(i) that most of the wave function is reflected back and propagates back towards the initial position.

In other words most of our wave function cannot overcome the potential high wall that is set up in the middle of the $xy$ grid, thus they are bounced backed,

while for some quantum physical reason, some of the wave function do end up being on the other side of the wall.

### 4.3 The Detection Probability along a detector screen

We measure the particle with a detector screen at $x = 0.8$, which spans the entire $y$ axis at time $t = 0.002$. We assume that we do indeed detect the particle somewhere along this screen. By plotting $p(y|x = 0.8; t = 0.002)$, we see the following pattern for each slit configuration.

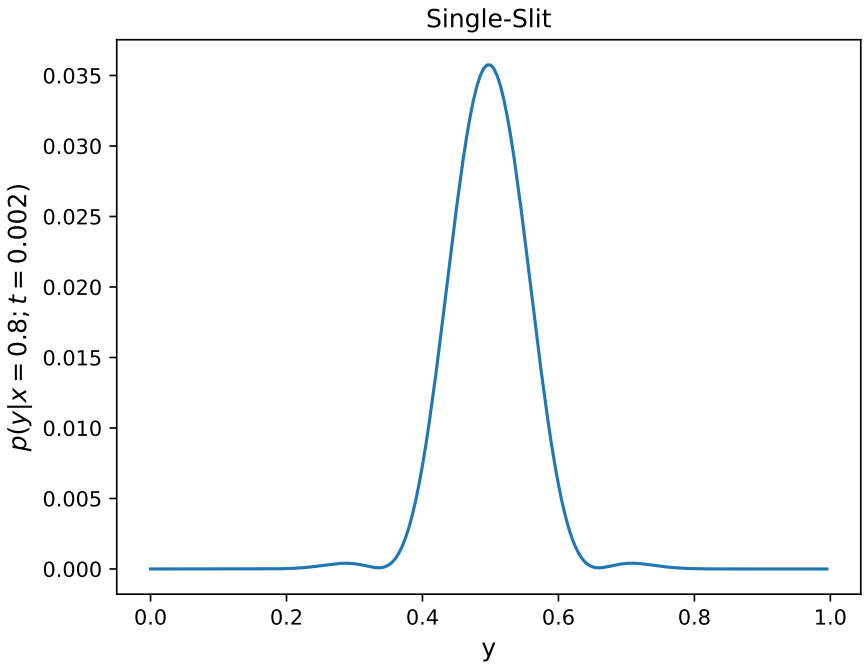


Figure 6: 1D probability observed from a span in the y-axis for single slit configuration. This figure shows us a single particle simulation through a single-slit is

We observe a single particle in a position of $x = 0.8$ at time $t = 0.002$. From that point of view, we observe the span along the y axis and how the particle acts like a single wave when it slits through the single slit. By observing the top of the function we can say that this is the detection of a single particle moving through a single-slit.

By creating a single split probability plot along the y axis, we see a top in the middle. This top is caused by a single wave passing through the slit.

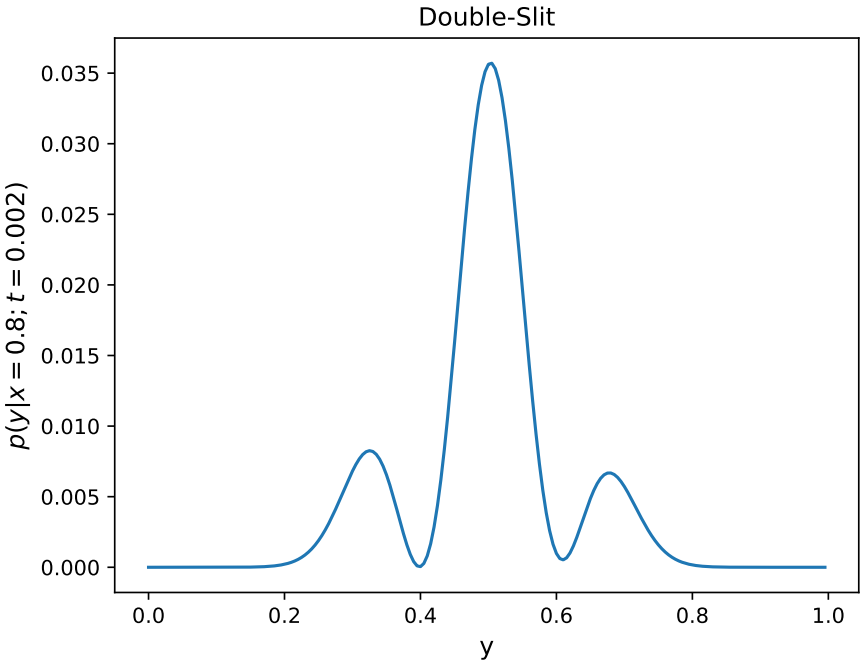


Figure 7: 1D probability along the y-axis for double slit configuration

Compared to that of the single slit we now see there are two extra tops in the graph this comes from the waves now overlapping each other and creating constructive interference in the two parts slit. This is caused by the maximum of of two waves adding up and creating a bigger amplitude in the wave function.

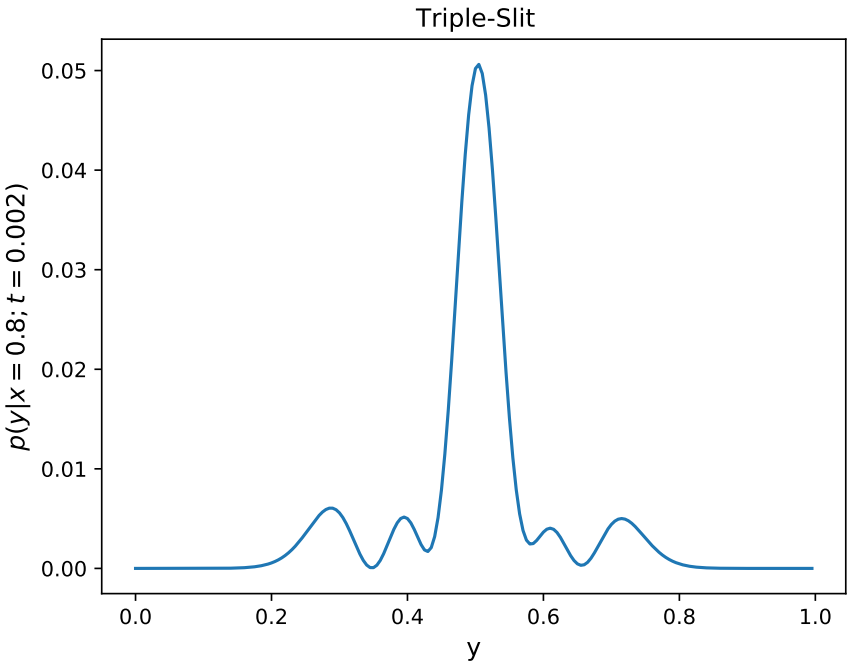


Figure 8: 1D probability along the y-axis for triple slit configuration

The same situation for the double slit in (7) applies to the triple slit, as this leads to more overlap of the waves creating more constructive interference. With three slits we derive more tops as the waves pass through the barrier.

# 5 Conclusion

In this article, we have simulated the two-dimensional time dependant Schrödinger equation of dimension 2+1 and then used this to study both non-slit barrier and multiple-slit barriers. We used Crank Nicolsons method on the Schrödinger equation to integrate and find the wave function $u_{ij}^n$ for $t = n$. Through this, we were able to do a consistency check by plotting the total probability of the system. We found that Crank Nicolsons method is a accurate method to implement when simulating a partial differential time dependant equation. However, small deviations were observed from the true value 1. These deviations, as discussed, were mainly caused by the way the matrix equation 2.2.1 was solved.

In like manner the 2D probability function $p_{ij}^n$, as well as the colourmap plots of the real and imaginary part of the wave function $u_{ij}^n$ at specified times steps were plotted. This enabled further observations of the nature of the simulation, such as the diffraction of the wave.

Furthermore the 1D probability function at $x = 0.8$ in time $t = 0.002$ was plotted as a function of the $y$-axis to see the detection probability distribution along this line. As expected it showed a diffraction pattern for all slit-in-a-box configuration.

A future improvement to this simulation would be to utilize another numerical method to solve the matrix equation 2.2.1, and compare which method gives a more accurate result. Potentially, iterative methods could increase efficiency and accuracy of solving the matrix equation needed in the Crank Nicolson method considering we are working with sparse matrices $A$ and $B$.

# References


[1] S. J. Axler, *Linear algebra done right*. Springer, 1997, vol. 2. [Online]. Available: `https://link.springer.com/content/pdf/10.1007/978-3-319-11080-6.pdf`.

[2] F. Galbusera and F. Niemeyer, "Chapter 14 - mathematical and finite element modeling," in *Biomechanics of the Spine*, F. Galbusera and H.-J. Wilke, Eds., Academic Press, 2018, pp. 239–255, ISBN: 978-0-12-812851-0. DOI: `https://doi.org/10.1016/B978-0-12-812851-0.00014-8`. [Online]. Available: `https://www.sciencedirect.com/science/article/pii/B9780128128510000148`.

# A Appendix

## A.1 Analytical discretizised equation of the "bare" Schrödinger equation.

We start of with the "bare" equation:

$$i\frac{\partial u}{\partial t} = -\frac{\partial^2 u}{\partial x^2} - \frac{\partial^2 u}{\partial y^2} + v(x,y)u, \tag{11}$$

We discretize the equation :

$$\begin{aligned} x \to x_i = ih, \text{ with } i = 0, 1..., M-1, \\ y \to y_j = jh, \text{ with } j = 0, 1..., M-1, \\ u(x,y,t) \to u(ih, jh, \Delta t) = u_{ij}^n, \\ v(x,y) \to v(ih, jh) \equiv v_{ij}. \end{aligned}$$

We then make an approximation: $\frac{\partial u}{\partial t} = -\frac{\partial^2 u}{\partial x^2} - \frac{\partial^2 u}{\partial y^2}$

$$\begin{aligned} \frac{u_{i,j}^{n+1} - u_{i,j}^n}{\partial t} = -\frac{1}{2}\Big[\frac{u_{i+1,j}^{n+1} - 2u_{i,j}^{n+1} + u_{i-1,j}^{n+1}}{(ih)^2} + \frac{u_{i+1,j}^n - 2u_{i,j}^n + u_{i-1,j}^n}{(ih)^2}\Big] \\ -\frac{1}{2}\Big[\frac{u_{i,j+1}^{n+1} - 2u_{i,j}^{n+1} + u_{i,j-1}^{n+1}}{(jh)^2} + \frac{u_{i,j+1}^n - 2u_{i,j}^n + u_{i,j-1}^n}{(jh)^2}\Big], \end{aligned}$$

We then make an approximation of the potential:

$$v(x,y)u = \frac{1}{2}\Big[v_{i,j}^{n+1}u_{i,j}^{n+1} + v_{i,j}^n u_{i,j}^n\Big], \tag{12}$$

We then collect $n+1$ and $n$ on each side of the equal sign:

$$u_{i,j}^{n+1} - r[u_{i+1,j}^{n+1} - 2u_{i,j}^{n+1} + u_{i-1,j}^{n+1}] - r[u_{i,j+1}^{n+1} - 2u_{i,j}^{n+1} + u_{i,j-1}^{n+1}] + \frac{i\Delta t}{2}v_{i,j}^{n+1}u_{i,j}^{n+1} \tag{13}$$

$$= u_{i,j}^n - r[u_{i+1,j}^n - 2u_{i,j}^n + u_{i-1,j}^n] - r[u_{i,j+1}^n - 2u_{i,j}^n + u_{i,j-1}^n] + \frac{i\Delta t}{2}v_{i,j}^n u_{i,j}^n. \tag{14}$$

Where $r = \frac{i\Delta t}{2h^2}$.